Mathematical Modeling and Experimental Identification of a Model Helicopter*

S. K. Kim† and D. M. Tilbury‡
Department of Mechanical Engineering and Applied Mechanics
University of Michigan, 2250 G.G. Brown, 2350 Hayward St.
Ann Arbor, MI 48109-2125
{sungk,tilbury}@umich.edu

Submitted to the AIAA Journal of Guidance, Control, and Dynamics
August 31, 2000

Abstract

This paper presents a new mathematical model for a model-scale helicopter. Working from first principles and basic aerodynamics, the equations of motion for full six degree-of-freedom motion are derived. The control inputs considered are the four pilot commands from the radio transmitter: roll, pitch, yaw, and thrust. The model helicopter has a fast time-domain response due to its small size, and is inherently unstable. Most commercially available model helicopters use a flybar to augment stability and make it easier for a pilot to fly. The main contribution of this paper is to model the interaction between the flybar and the main rotor blade; it is shown how the flapping of the flybar increases the stability of the model helicopter as well as assists in its actuation. This model can better predict the response of the helicopter than a simple linear model. After the mathematical model is derived, system identification experiments and results are presented to verify the mathematical model structure and to identify model parameters such as inertias and aerodynamic constants.

1 Introduction

It has been more than 20 years since the first commercial model helicopter was built, and since then, the design has significantly improved. Model helicopters are now well within the reach of many hobbyists and are also often used for commercial purposes, such as crop dusting or sport-event broadcasting. However, model helicopters are inherently unstable. Even with improved stability augmentation devices, a skilled, experienced pilot is required to control them during flight. Despite such difficulties, as a small, dynamically fast, unstable system, a model helicopter makes an excellent testbed for nonlinear control.

This paper describes the new mathematical model that we have derived specifically for a model helicopter, as well as the system identification experiments we have conducted. The model is based on a rigid-body

*This research was supported in part by the Michigan Space Grant Consortium, the Rackham Graduate School, and the NSF under grant numbers IRI 95-28115 and CMS 98-76039.

†Ph.D. Student, AIAA Student Member

‡Assistant Professor

description of the helicopter, with four actuation inputs representing the four stick positions available to the remote-control pilot. The main contribution of the paper is the detailed modeling of the actuator dynamics, including the interaction of the flybar with the main rotor blade, which increases the stability of the model helicopter. Once the mathematical model has been developed, system identification experiments are performed both to verify the structure of the model and to identify some of the unknown model parameters, such as inertias and aerodynamic coefficients.

The outline of the paper is as follows. First, we briefly review some previous work on helicopter modeling and control. In section 3, we describe the new mathematical model that we have derived, working from first principles and basic aerodynamics. Section 4 describes the system identification technique for identifying the uncertain parameters and presents our results. We end with the validation of our derived model which compares the model with experimental hover data.

2 Related Work

2.1 Mathematical Modeling

A number of researchers have devised a mathematical model of a model helicopter based on the basic structure of a full scale helicopter. Lee et al. [14] devised a linear 6DOF model based on a hovering helicopter with a flapping rotor, using equations for a full-scale helicopter. Based on this model, regulation of the 3DOF motion (roll, pitch, and yaw) were performed using a digital LQG controller on a model helicopter fixed on a stand. The validity of the model was not investigated through a full 6DOF hover experiment.

Furuta et al. [7] derived a mathematical model of a model helicopter fixed on a stand, free to rotate around the pitch, roll, and yaw axis. Realizing that the model helicopter is hard to control manually, a stable tracking controller was designed using state space methods. This stabilizing control input is then used to compare and validate the derived mathematical model with the experimental result. The model they derived was based on the full-scale helicopter modeling, including a flapping rotor hub with spring.

Azuma [3] from University of Tokyo derived a mathematical model of a rigid rotor system. In this rotor system, each rotor blade is hinged but is spring loaded. He carefully derived a equation of motion considering how different flapping stiffness affects the response of the system. Since this model does not take into account the dynamics of the helicopter as a whole, the validity of the model has not been fully proven. The model is also geared toward full scale rotor design.

At Purdue [20], a student derived the dynamic equation of a model helicopter's vertical motion using blade element theory. For the experiment, a model helicopter was affixed to a stand and restricted to vertical motion. Unknown parameters were estimated by interpolating the results from a number of experiments at different operating points. The experiment was not extended to include other degrees of freedom.

Meanwhile, the annual unmanned aerial vehicle competition [5] has been organizing a number of universities to complete a task of recognizing and moving an object to a designated target. Thus far, the competitors have been focused on the sensory issues such as the image processing, with a lesser emphasis on the modeling and control problems.

The MIT, Boston University and Draper Lab team [11, 10] was successful in building an autonomous model helicopter designed to hover, fly around, and recognize five randomly placed drums during the 1996 International Aerial Robotics Competition. The system consisted of the helicopter with various sensors such as GPS, IMU, altimeter, and compass, as well as a ground control station, a vision processor, and a safety

pilot. A simplified mathematical helicopter model with a flapping rotor and first order linear flybar model is used for guidance, navigation, control analysis, and training. Simulation was used extensively to save development time and cost. The use of the simplified model presented could limit the ultimate performance of the designed controller, especially if more aggressive or fast maneuvers are desired.

Weilenmann and Geering [27] devised a 6DOF stand for a model helicopter with 3 spring-loaded arms with 3 joints for each arm. The author claims the kinematics of the stand cannot be given analytically, but the stand is almost equivalent to a point mass attached to the helicopter. A 6DOF, 18th order linear state space model with flybar dynamics is also presented. A satisfactory 6DOF hover experiment was obtained through LQG/LTR controller based on the linear model. The paper is sketchy about the performance and the detail of the linear model which limited the potential of using the model for other model-scale helicopters. The role of the stand to the dynamic response of the helicopter also needs to be explained.

2.2 Empirical Approaches

Researchers at Caltech [16, 28] attempted to capture the main dynamic features of a model helicopter near hover with a linear time-invariant model. A MIMO identification algorithm was used to account for the significant cross-couplings in the model helicopter. A model helicopter was fixed on a stand to provide three degrees of freedom: pitch, roll, and yaw rotations. Translational movements such as x, y, and z positions were neglected. The identification was carried out using a quadratic weighing factor with an iterative Gauss-Newton algorithm. The match between simulation and experiment was good in the pitch and roll directions, but was poor in the yaw direction due to the actuation asymmetry. Since the model is strictly based on the numerical identification, possible nonlinear behavior of the rotor system is not taken into account.

Teare et al. [26] did identification for UH-60 helicopter with a linearized 6DOF general model based on a 6DOF Euler equation using the least squares and the maximum likelihood method. The external forces and moments were assumed to be functions of the inputs and velocity states. As the result of linearization, terms such as a derivative of a force with respect to an input are the parameters to be identified. No analytic modeling is applied to the model. The ID results were verified only by comparing the "energy" of the the state derivatives and the error signal without graphical comparison. The author emphasized the importance of using a priori knowledge about the model parameters being identified in order to design flight test inputs that provide proper excitation.

Rohlfs [22] did identification for a Bo 105 helicopter with a nonlinear 9DOF model including 6DOF rigid body dynamics and 3DOF flapping rotor dynamics using the maximum likelihood method. Over 100 derivative parameters were identified successfully by improving the data quality via comparing redundant measurements and careful visual inspection. Regarding the mathematical model, force and moment expressions were based on the linear combination of most states and unknown derivatives to be identified, making the model essentially a black-box. Because of this, it is unclear how physically meaningful each identified parameter is when compared to an existing purely analytical model.

Sugeno [25] has had a considerable amount of success in flying a model helicopter for commercial purposes. The control system was designed using fuzzy control theory. The integrated control system, ranging from low level basic flight modes to high level supervisory control, takes a human voice as its input.

Montgomery and Bekey from USC [15] developed an automatic controller for pitch and roll motion using model-free fuzzy logic and a neural network. As most other fuzzy logic controller, the performance of the controller is only good for certain types of tasks or objectives.

3 Mathematical model

Although a model helicopter may seem just a miniaturization of a full-scale version, there are significant differences between the two. The first major difference between model and full-scale helicopters has to do with the rotor configuration. Many full scale helicopters have a hinge, either free-flapping or spring-mounted, on the rotor blades, so that the plane of the rotor can be tilted with respect to the helicopter. Such a hinge system allows the rotor blades to flap, increasing the stability. However, this flapping behavior increases the time needed for the helicopter to respond to control inputs. By tilting the rotor disc forward, the helicopter can move forwards while remaining level [12]. Most model helicopters have a hingeless, stiff rotor hub design, which forces the position of the fuselage to remain fixed with respect to the rotor disc. This results in faster response times, and gives the remote pilot a better sense of motion of the helicopter. However, in order to move forwards, a model helicopter must first pitch forwards, giving a forward component to the main thrust vector.

Secondly, the stability properties are quite different. The time-domain response of a model helicopter is much faster due to its small size. Without any extra stability augmentation devices, a human pilot would have difficulty controlling it. In most model helicopters, a large control gyro with an airfoil, referred to as a *flybar*, is used to improve the stability characteristic around the pitch and roll axes and to minimize the actuator force required. The flybar modeling will be presented in Section 3.4. In addition, an electronic gyro is used on the tail rotor to further stabilize the yaw axes. In most full scale helicopters, the large rotor and fuselage inertias and the flapping rotor hinge provide adequate stability, and extra control gyros on the rotors are unnecessary.

Because of these significant differences, a mathematical model for a model helicopter cannot just be a scaled-down version of a full-scale model; the different actuation mechanisms must be taken into account. In this section, we derive the dynamic equations of motion for the model helicopter including its actuator dynamics. The equations are based on rigid body dynamics [17], as well as basic aerodynamics and helicopter theory [12, 19]. Once the structure of the model has been determined, system identification techniques will be used to validate the model and determine the unknown model parameters.

As shown in Figure 1, our modeling is based on a commercially available model helicopter called Ikarus [8]; most other brands of model helicopters have a similar structure. It has a 1.02 m rotor span, and weighs 1.36 kg without the onboard battery. A sensor is attached to the tail fin to measure the position and orientation of the helicopter with respect to an inertial frame. Figure 2 shows some of the onboard components, including a radio receiver which receives command inputs from the remote control box, a motor with a motor controller, four different servos (pitch and roll cyclic, collective pitch, and yaw servo), and a gyro sensor. The single electric motor drives the main and tail rotors simultaneously, and the gyro sensor on the tail rotor is used by the yaw servo to give extra damping to the yaw control.

3.1 Coordinates and Frames

As shown in Figure 3, there are two frames that we consider: the reference inertial frame, and the body frame attached to the helicopter. The transformation between the two frames is given by the homogeneous

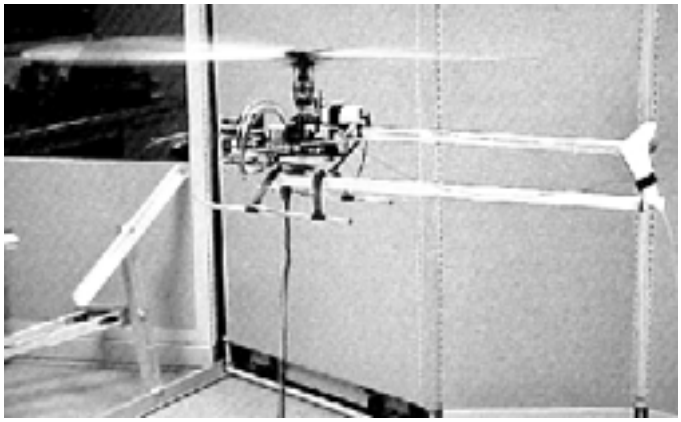

Figure 1: A photograph of the Ikarus ECO electric helicopter used in our experiment [8]. The sensor receiver is attached to the tail to minimize the electromagnetic interference from the motor. The sensor transmitter is fixed to the ground, although different locations were chosen to minimize the distance between the transmitter and receiver depending on the nature of experiment. Because the sensor arrangement already requires the helicopter to be tethered, we power the helicopter motor using a 12V car battery.

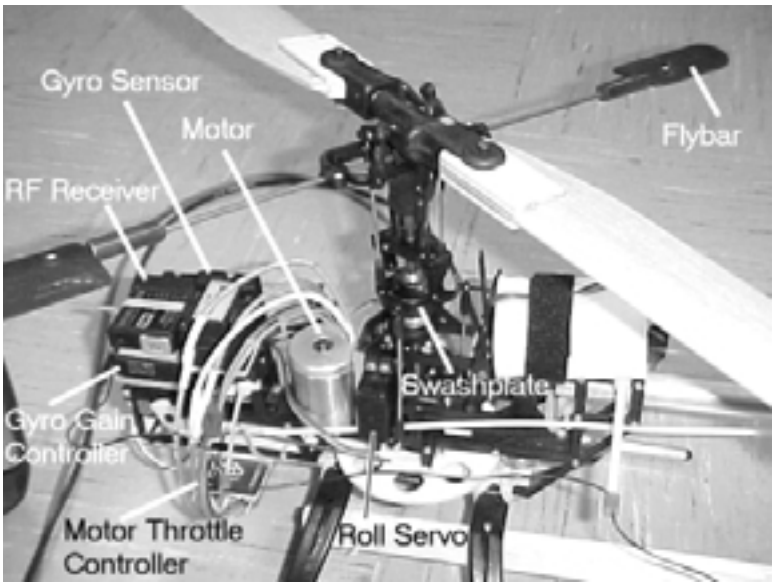

Figure 2: Some of the mechanical and electrical components on the helicopter. A minor reduction in sensor noise was obtained using a brushless motor [2]. All other components are generic model helicopter components.

transformation matrix

$$g_{IB} = \begin{bmatrix} & & & x_I \\ & R_{IB} & & y_I \\ & & & z_I \\ 0 & 0 & 0 & 1 \end{bmatrix}$$

where the rotation matrix R_{IB} represents the relative orientation between the two frames. The rotation matrix can be expressed in coordinates using yaw-pitch-roll (ZYX) Euler angles as:

$$\begin{aligned} R_{IB} &= e^{(\hat{\mathbf{z}}\times)\psi} e^{(\hat{\mathbf{y}}\times)\theta} e^{(\hat{\mathbf{x}}\times)\phi} \\ &= \begin{bmatrix} \cos\psi & -\sin\psi & 0 \\ \sin\psi & \cos\psi & 0 \\ 0 & 0 & 1 \end{bmatrix} \cdot \begin{bmatrix} \cos\theta & 0 & \sin\theta \\ 0 & 1 & 0 \\ -\sin\theta & 0 & \cos\theta \end{bmatrix} \cdot \begin{bmatrix} 1 & 0 & 0 \\ 0 & \cos\phi & -\sin\phi \\ 0 & \sin\phi & \cos\phi \end{bmatrix} \end{aligned}$$

Although this representation is singular at $\theta = \pm\pi/2$, we do not expect to operate the helicopter in that orientation (pointing straight up or down). Thus, we will do most of our derivation in coordinates, where (x_I, y_I, z_I) are the coordinates of the position of the helicopter with respect to the inertial frame and ϕ, θ, ψ are the Euler angles of the helicopter with respect to the inertial frame.

There are several different velocities that will be used to write the dynamic equations. The linear velocity of the helicopter with respect to the inertial frame is $v_I = \begin{bmatrix} \dot{x}_I & \dot{y}_I & \dot{z}_I \end{bmatrix}^T$. This velocity can also be expressed in the body frame,

$$v_B = R_{IB}^T v_I$$

The angular velocity of the helicopter will also be needed. The angular velocity of the helicopter with respect to the inertial frame, expressed in the body frame, is denoted ω_B and can be computed as

$$\begin{aligned} \omega_B \times &= R_{IB}^T \dot{R}_{IB} \\ \omega_B &= \begin{bmatrix} \dot{\phi} - \dot{\psi}\sin\theta \\ \dot{\theta}\cos\phi + \dot{\psi}\cos\theta\sin\phi \\ -\dot{\theta}\sin\phi + \dot{\psi}\cos\theta\cos\phi \end{bmatrix} = \begin{bmatrix} 1 & 0 & -\sin\theta \\ 0 & \cos\phi & \cos\theta\sin\phi \\ 0 & -\sin\phi & \cos\theta\cos\phi \end{bmatrix} \begin{bmatrix} \dot{\phi} \\ \dot{\theta} \\ \dot{\psi} \end{bmatrix} \end{aligned} \tag{1}$$

3.2 Rigid Body Equations

We will model the helicopter as a rigid body moving in space, ignoring the effects of the spinning rotor. Although this is not physically true, this assumption helps us to collect all the various inertia effects such as main and tail rotor dynamics into a simple constant mass-inertia matrix. This assumption will be justified through the system identification in Section 4. The mass of the helicopter is given by m, and the fuselage inertias are I_{xx}, I_{yy}, I_{zz}. The inertia matrix $\mathcal{I}$, in body coordinates, is :

$$\mathcal{I} = \begin{pmatrix} I_{xx} & 0 & -I_{xz} \\ 0 & I_{yy} & 0 \\ -I_{xz} & 0 & I_{zz} \end{pmatrix}$$

Terms such as I_{xy} and I_{yz} are zero due to the symmetry of the helicopter with respect to the x_B-z_B plane. Although I_{xz} is non-zero, because the helicopter is not symmetric with respect to the x_B-y_B plane, it is typically much smaller than the other terms. We will ignore it in our model.

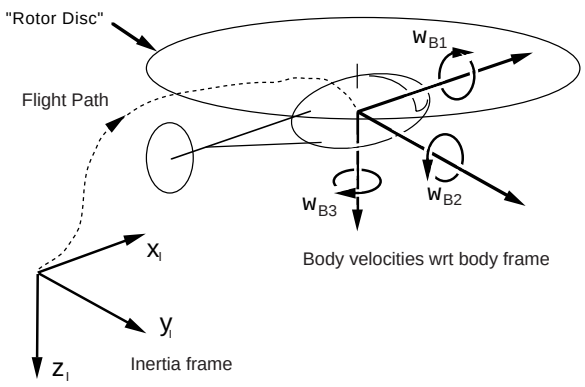

Figure 3: The coordinates defined. The inertial frame is fixed to the ground, and the body frame is fixed to the helicopter. The relative rotation between the two frames is given by the rotation matrix R_{IB}, or equivalently by the ZYX Euler angles (ϕ, θ, ψ), and the relative displacement is given by the vector $[x_I \quad y_I \quad z_I]^T$. The rotor disc is an imaginary plane drawn by the tip of main rotor blades.

The dynamic equations of the helicopter's motion are significantly simplified by expressing them in body coordinates. In these coordinates, Euler's equations for the rigid body motion of the helicopter become [17]

$$\begin{bmatrix} m\, I_{3\times 3} & 0 \\ 0 & \mathcal{I} \end{bmatrix} \begin{bmatrix} \dot{v}_B \\ \dot{\omega}_B \end{bmatrix} + \begin{bmatrix} \omega_B \times m v_B \\ \omega_B \times \mathcal{I}\omega_B \end{bmatrix} = \begin{bmatrix} f_B \\ \tau_B \end{bmatrix} \tag{2}$$

The external forces and torques expressed in the body frame are f_B and τ_B. The body force f_B includes aerodynamic drag terms D_F, the main and tail rotor thrusts T and T_T, and the gravitational force mg.

$$f_B = \begin{bmatrix} -D_{F_x} \\ -D_{F_y} - T_T \\ -D_{F_z} - T \end{bmatrix} + R_{IB}^T \begin{bmatrix} 0 \\ 0 \\ mg \end{bmatrix} \tag{3}$$

Torques include the three main directional torques M_ϕ, M_θ, M_ψ as well as a torque due to the offset of the rotor hinge $T\ell_r$, and the motor torque τ_m.

$$\tau_B = \begin{bmatrix} M_\phi \\ M_\theta - T\ell_r \\ M_\psi + \tau_m \end{bmatrix} \tag{4}$$

The longitudinal offset between the rotor axis and the helicopter's center of gravity is ℓ_r. Usually this offset is expected to be small for better handling quality. Nevertheless, we will assume this quantity is non-zero for generality. The gravitational acceleration constant is g. It is assumed that the helicopter's center of gravity is in-line with the rotor axis laterally, because most components such as motor and gear trains are located along the x_B-z_B plane, with y_B near zero.

The four independent inputs to this model are T, the net thrust generated by the rotor, and M_ϕ, M_θ, M_ψ, the net moments acting on the helicopter. These four inputs are physically controlled by two joysticks on the radio transmitter, each with two degrees of freedom. The left joystick commands throttle with collective pitch (up/down) and yaw (left/right), and the right joystick commands pitch cyclic (up/down) and roll cyclic (left/right). This is the most popular configuration used in the U.S. (type II[1]). The four values representing

[1]In some countries, people prefer the yaw and the roll controls switched (type I).

the positions of the sticks are encoded in a pulse-width modulated (PWM) signal, and sent via radio link to the helicopter.

To match with our experimental measurements, we will also consider the transformation of the Newton-Euler equation (2) into a new set of coordinates, q, which includes the inertial position and velocity of the helicopter, the Euler angles, and the body angular velocity [13]:

$$q = \begin{bmatrix} x_I & y_I & z_I & \dot{x}_I & \dot{y}_I & \dot{z}_I & \phi & \theta & \psi & \omega_{B1} & \omega_{B2} & \omega_{B3} \end{bmatrix}^T$$

The transformed equations become

$$\dot{q} = \begin{bmatrix} v_I \\ \frac{1}{m} R_{IB} f_B \\ \Upsilon \, \omega_B \\ \mathcal{I}^{-1}(\tau_B - \omega_B \times \mathcal{I} \, \omega_B) \end{bmatrix} \tag{5}$$

where Υ is the inverse of the matrix shown in (1):

$$\Upsilon = \begin{bmatrix} 1 & 0 & -\sin\theta \\ 0 & \cos\phi & \cos\theta\sin\phi \\ 0 & -\sin\phi & \cos\theta\cos\phi \end{bmatrix}^{-1} = \begin{bmatrix} 1 & \sin\phi\tan\theta & \cos\phi\tan\theta \\ 0 & \cos\phi & -\sin\phi \\ 0 & \sin\phi\sec\theta & \cos\phi\sec\theta \end{bmatrix}$$

Note that this expression highlights the singularity of the representation at $\theta = \pm\pi/2$.

3.3 Aerodynamic modeling

Before developing the actuation equations, we introduce some basic aerodynamic terms that will be required. We will assume the rotor system is completely rigid (there is no aeroelasticity effect), and that the airfoil is symmetric and non-twisted. The aerodynamic interaction between the rotor and the fuselage is neglected. The aerodynamic expressions are based on 2-D analysis. This type of modeling is often called level-1 modeling and is appropriate for low bandwidth control and to observe the parametric trends for flying qualities and performance studies [19].

The rotor span, R is assumed to be the distance between the rotor axis and the rotor tip. We neglect the effect due to "root cutout," where there is no rotor blade at the hub area [12]. The model helicopter's rotor blade remains nearly rigid due to its short length (0.4 to 0.8 meter), high rotor speed (1200 to 1900 rpm), and hingeless hub design; we assume the rotor is perfectly rigid with no twist.

The descent ratio, ν, represents the air speed component perpendicular to the rotor disc [18]. To define it, we first need to find the velocity of the hub point with respect to the inertial coordinate frame represented in body coordinates; we denote this velocity by v_q^b. The coordinate of the rotor hub point in the body frame is $q_b = [\ell_r \;\; 0 \;\; -h_r]^T$. The constants $-h_r$ and ℓ_r are the offsets of the rotor from the helicopter's center of gravity in the x_B and z_B directions respectively; the rotor hub is in-line with the center of gravity in the y_B direction.

$$v_q^b = \omega_B \times q_b + v_B \tag{6}$$

The descent ratio, ν, which is the airspeed component perpendicular to the rotor disc, can be found as the magnitude of the third element of v_q^b, non-dimensionalized by $R\Omega$.

$$\nu = \frac{1}{R\Omega} v_{q3}^b \tag{7}$$

When the helicopter is hovering, this ratio will be very small and may be ignored. The inflow ratio, λ, is the net value of the descent ratio ν and the induced air velocity. The velocity of the air through the rotor blade v_i, is defined to be positive when the flow is along the z_B-axis, and is non-dimensionalized by $R\Omega$. We choose not to model λ in any more detail in this paper due to its inherent complexity [12].

$$\lambda = -\nu + \frac{v_i}{R\Omega} \tag{8}$$

The most important parameter in determining the lift force is the angle of attack of a blade, which is the angle between the centerline of the blade and the blade velocity vector with respect to the inertial frame. The angle of incidence, which is the angle between the centerline of the blade and the reference frame (such as the rotor axis), is not related to the aerodynamic effects. The lift curve slope, a is the slope of the function of the lift force vs. angle of attack of the main rotor blade [24]; we assume here that a is a constant.

3.4 Flybar dynamics

The dynamics of the rotor and the flybar are the most significant nonlinearities involved in the creation of the forces and moments on the helicopter. The actuator dynamics include as states the flapping angle and velocity $(\beta, \dot{\beta})$ of the flybar and the position and angular velocity (ξ, Ω) of the main rotor blade. As mentioned before, the flybar plays a major role in augmenting the stability of a model helicopter. The flybar mechanism is sketched in Figure 4. The original concept of this design came from full-scale helicopter stabilization devices first used in the 1950s. The Bell stabilizing system had a bar with weights at each end, and the flapping motion of the bar was governed by a separate damper. The Hiller system replaced the damper and the weights with an airfoil. During the early 1970s, the design was simplified and improved for model-scale helicopters [23]. This system is often called a Bell-Hiller mixer, because it incorporates some of design aspects of both Bell and Hiller designs. The fundamental concept for the model helicopter's rotor hub design is identical to the Hiller system, although the mechanical detail resembles the Bell system. Since the early 1970s, the design of the model helicopter's rotor hub has gone through many changes and improvements; it reached its current state in the early 1990s. The rotor hub design presented in Figure 4, hingeless with Bell-Hiller mixer, represents currently the most popular and widely accepted design as the best compromise between performance and stability. However, it is suited more toward aerobatic maneuvers than smooth near-hover maneuvers that do not require large and fast pitch or roll movements. Stability can be increased if the Bell input is removed and/or the main blade is allowed to flap, but the helicopter would then respond more slowly [23].

Figure 4 shows the two arms coming from the swashplate. One arm, marked Bell input, allows the blade pitch to be changed directly from the cyclic servo actuator. The response with respect to this arm alone is fast, but lacks stability. Meanwhile, the other arm, marked Hiller input, allows the pitch of the flybar to be changed. The flybar then flaps, and this flapping motion causes the pitch of the main blade to change. The pilot's cyclic control input δ_θ and δ_ϕ are the displacements of the lower swashplate as per Figure 4. There is a direct relationship between the cyclic input applied to the main blades δ_{cyc} (which is a function of δ_θ and δ_ϕ) and the cyclic angle of the rotor blades θ_{cyc}. A similar relationship exists between the cyclic input applied to the flybar δ_{fly} and the flapping angle of the flybar β. The orientation of the main blade with respect to the helicopter is given by ξ. The factor L_8/L_9 reflects the different diameters of the upper and lower swashplates. Note the 90° phase difference between δ_{cyc} and δ_{fly}, due to the geometry of the

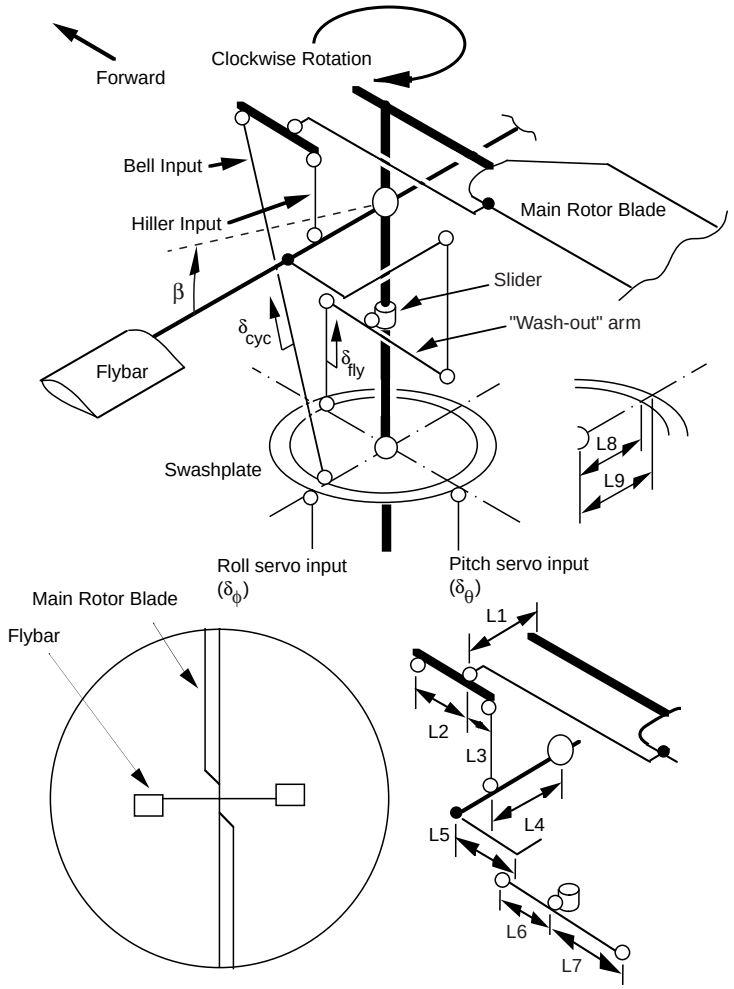

Figure 4: The basic structure of the model helicopter's cyclic/collective control system. Only one side of the assembly is shown for clarity; the other is simply a mirror image. The flapping angle of the flybar, β, is the angle of the flybar with respect to the body coordinate frame attached to the rotor hub. It is zero when the flybar is perpendicular to the rotor axis. Ball joints are shown as "$\circ$", and fixed joints are shown as "$\bullet$". The cyclic pitch input to the main rotor blade is controlled by the combination of the Bell input from the swashplate and the Hiller input from the flybar. The collective pitch input to the main rotor blade is controlled by raising or lowering the swashplate. The "wash-out" arm with the slider prevents the collective input from affecting the flybar. The flybar angle of incidence and the flapping angle are thus separated from the collective input. The slider slides only when the collective input is applied. The slider remains stationary when only a cyclic input is applied.

rotor/flybar assembly shown in Figure 4.

$$\delta_{cyc}(\xi) = -\frac{L_8}{L_9}(\delta_\theta \sin\xi + \delta_\phi \cos\xi) \tag{9}$$

$$\delta_{fly}(\xi) = -\frac{L_8}{L_9}(\delta_\theta \cos\xi - \delta_\phi \sin\xi) \tag{10}$$

An important assumption at this point is that the rotor system does not apply reaction forces back to the actuators, including the flybar (the flybar is considered to be another actuator to the main blades). This is equivalent to assuming the actuators are able to apply infinite amount of forces to the airfoils. This assumption is reasonable because the airfoil of the main blades is symmetric and the blades are hinged along the center of lift. Ideally, the moment required to rotate the blade at this point should be very small [24].

When a cyclic input is applied by the pilot, the flybar creates lift which tilts the flybar disc. The flybar acts not only as a main blade angle actuator but also as a stabilizer. If the cyclic input were applied to the main blades only, large control forces on the cyclic servo actuators would be required [9]. By applying the cyclic control to the flybar and allowing the flybar to apply a secondary cyclic input to the main blade, the servo load is significantly reduced.

The flybar is hinged on the main axis to flap freely and rotate around the main axis while remaining 90° out of phase with respect to main blades. Therefore, its yaw angle with respect to the body frame is $\xi' = \xi + \pi/2$. Its flapping (pitching) angle, β, is measured with respect to the plane perpendicular to the main rotor axis. The roll motion of the flybar changes the angle of attack of the flybar, θ_{fly}. However, one can safely neglect the contribution of this motion in deriving an expression governing β, because of the flybar's small inertia. The roll motion of the flybar only affects the lift created by changing the angle of incidence of the main rotor blades. The rotation matrix which relates the flybar position to the body coordinates of the helicopter is denoted R_{BF}; that is,

$$R_{BF} = e^{(\hat{z}\times)(\xi')}\ e^{(\hat{y}\times)\beta}\ e^{(\hat{x}\times)0}$$

As before, the rotation matrix between the helicopter body frame and the inertial frame is R_{IB}. The rotation matrix relating the flybar frame to the inertial frame is thus the product of the two: $R_{IF} = R_{IB}R_{BF}$.

The rotational inertia of the flybar $\widehat{I}$ is unified as I_f; this is a reasonable assumption because most of the flybar mass is concentrated at the tip region. There are n rotor blades (in our helicopter, n=2).

$$I_f = n\int_{R_1}^{R_2} r^2\, m_F\, dr$$

$$\widehat{I} = \mathrm{diag}\begin{bmatrix} 0 & I_f & I_f \end{bmatrix}$$

The angular velocity of the flybar ω_F involves the velocity of the flybar and the helicopter simultaneously; it can be found by computing $R_{IF}^T \dot{R}_{IF}$ [17].

$$(\omega_F\times) = R_{IF}^T\dot{R}_{IF} = R_{BF}^T(\omega_B\times)R_{BF} + R_{BF}^T\dot{R}_{BF} \tag{11}$$

$$\omega_F = \begin{bmatrix} -\omega_{B3}\sin\beta + \cos\beta(\omega_{B1}\cos\xi' + \omega_{B2}\sin\xi') \\ \omega_{B2}\cos\xi' - \omega_{B1}\sin\xi' \\ \omega_{B3}\cos\beta + \sin\beta(\omega_{B1}\cos\xi' + \omega_{B2}\sin\xi') \end{bmatrix} + \begin{bmatrix} -\dot{\xi}'\sin\beta \\ \dot{\beta} \\ \dot{\xi}'\cos\beta \end{bmatrix} \tag{12}$$

Note that the flybar velocity can be expressed as the contribution of the helicopter motion expressed in the flybar frame and the contribution of the flapping of the flybar. We will assume that the rotor angular velocity is constant; thus, $\dot{\xi}' = \dot{\xi} = \Omega$.

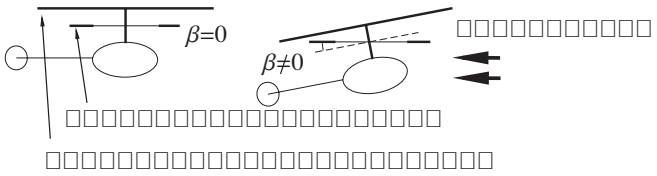

Figure 5: The stabilizing effect of the flybar. In a hovering situation, the flybar angle β is zero. If a wind gust or other disturbance knocks the helicopter out of its equilibrium, the flybar, which is hinged freely, will continue to rotate in the same inertial plane. Its angle with respect to the main blade becomes nonzero, and it will help bring the helicopter back to equilibrium through its action on the cyclic angle of the main blade.

The external moment applied to the flybar around the pitch axis is τ_{F2}; it is mainly created by aerodynamic lift. To find the total torque, we integrate along the length of the flybar. Since we will only be interested in the second of these three equations, we will not consider the first and the third elements in any detail.

$$\tau_F = \begin{bmatrix} \tau_{F_1} & n\int_{R_1}^{BR_2} r\, dL & \tau_{F_3} \end{bmatrix}^T \tag{13}$$

The constant tip loss factor B takes into account the fact that a finite length airfoil would lose some of the lift generated due to the wing tip vortex effect [12]. This effect is applied by "reducing" the length of the blade by the factor of B. Tip loss is often set to $B = 0.97$ [12].

The lift element dL depends on the angular velocity of the flybar and its angle of attack θ_{fly}. The angle of attack of the flybar will be influenced by the pilot input δ_{fly} and the ratio between the second element of the angular velocity vector of the flybar ω_{F2} and Ω [19]. Correction factors α_1 and α_2 have been included to compensate for the simplified aerodynamics; they will be identified experimentally in Section 4.

$$dL = \frac{1}{2}\rho(\Omega r)^2 a\, \theta_{fly}\, c_2\, dr \tag{14}$$

$$\theta_{fly} = \frac{\alpha_1 L_7}{L_5 L_6}\delta_{fly} - \frac{\alpha_2 \omega_{F2}}{\Omega} \tag{15}$$

Once the external force, angular velocity, and inertia have been defined, the motion of the flybar can be described using the Euler equation.

$$\tau_F = \omega_F \times \widehat{I}\,\omega_F + \widehat{I}\,\dot{\omega}_F \tag{16}$$

$$\begin{bmatrix} \tau_{F1} \\ n\int_{R_1}^{BR_2} r\, dL \\ \tau_{F3} \end{bmatrix} = \begin{bmatrix} 0 \\ -I_f\omega_{F1}\omega_{F3} \\ I_f\omega_{F1}\omega_{F2} \end{bmatrix} + \begin{bmatrix} 0 \\ I_f\dot{\omega}_{F2} \\ I_f\dot{\omega}_{F3} \end{bmatrix} \tag{17}$$

The second of these three equations describes the flapping motion of the flybar. The small angle approximation is used for β since it should not exceed about $\pm 25°$. For example, if roll motion only is considered, the second equation of (17) becomes the following.

$$\ddot{\beta} - \cos\xi\ddot{\phi} + 2\Omega\sin\xi\dot{\phi} - \sin^2\xi\beta\dot{\phi}^2 + \Omega^2\beta = \frac{n\Omega^2}{8}\frac{\rho a c_2(B^4R_2^4 - R_1^4)}{I_f}\left(\frac{\alpha_1 L_7 L_8}{L_5 L_6 L_9}\delta_\phi \sin\xi - \frac{\alpha_2(\dot{\beta} - \dot{\phi}\cos\xi)}{\Omega}\right) \tag{18}$$

The above expression is similar to the Bell stabilizing bar equation from a full-scale helicopter [4]. In the absence of aerodynamic forces and external moments, the flybar behaves as a gyroscope, maintaining

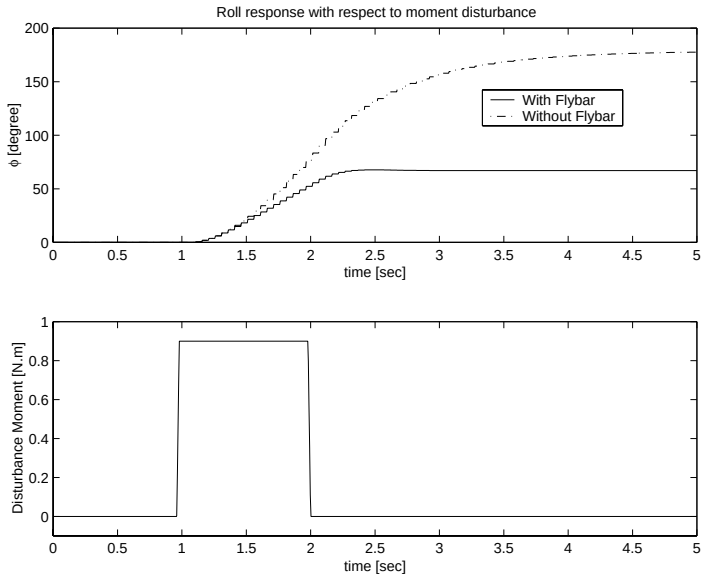

Figure 6: The roll response of the helicopter with respect to the roll moment disturbance are compared by simulation using the analytic model presented in Section 3.6. With the flybar, the response tends to settle within about 0.3 seconds. Simulating the no-flybar condition by setting $\beta = 0$, the helicopter reacts more strongly to the disturbance and takes longer to settle.

its orientation relative to inertial space [12], as shown in Figure 5. An external disturbance would upset the helicopter angles θ and ϕ, effectively changing β. This nonzero β acts to apply an appropriate compensation input to the main blade cyclic control system to stabilize the helicopter. Figure 6 compares the behavior of the model with and without the flybar.

3.5 Creation of Forces and Moments

Once the flybar dynamics have been found, the rest of the actuator dynamics can be derived. The four independent inputs to the rigid body dynamics are the thrust generated by the main rotor blade T, the moments created by the main rotor blade around the roll and the pitch axes (M_ϕ and M_θ), and the yaw moment M_ψ.

3.5.1 Main rotor thrust

The throttle/collective command δ_o controls the thrust to the main motor (T) as well as the collective pitch (θ_o) of the rotor blades. As the blade pitch increases, more lift is created, and the rotational motion of the main rotor blade is converted into vertical thrust. We define δ_o as the collective pitch angle measured when the helicopter is at rest. The mechanical linkages in the collective control system of Figure 4 introduce significant compliance; thus, a second-order mass-spring-damper model is used to model the actual collective pitch angle θ_o while flying.

$$\ddot{\theta}_o + K_5\dot{\theta}_o + K_6\theta_o = K_4 \cdot \delta_o \tag{19}$$

An adequate torque τ_m linked to δ_o is applied to keep Ω constant. Sometimes, an electronic throttle governor is used for this purpose, but mostly an empirical curve determining the necessary functional relationship

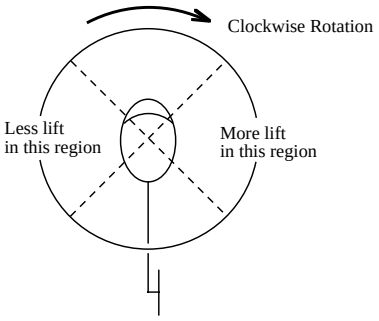

Figure 7: The top view of the helicopter. The lift distribution on the rotor disc when a forward cyclic (pitch forward) input is applied. The precession effect will pitch the helicopter forward.

between τ_m and δ_o is programmed into the radio transmitter.

The expression for the rotor thrust T near hover in terms of the collective pitch is obtained from [18].

$$T = \frac{n}{2} ac\rho\pi R^3\Omega^2 \left(\frac{B^3}{3}\theta_o - \frac{B^2}{2}\lambda \right) \tag{20}$$

This is an expression of the average thrust contribution about one revolution of the rotor blades; the average contribution of the cyclic pitch is zero.

3.5.2 Pitch and Roll moments

The pitch and roll commands vary the cyclic pitch (θ_{cyc}) of the rotor blades around each cycle of rotation, creating different amounts of lift in different regions (as shown in Figure 7). These differing amounts of thrust create a moment around the rotor hub, and can thus create pitch and roll moments on the helicopter.

The moment created by a roll cyclic input is derived by summing the forces around a revolution and along a rotor blade. As per Figure 7, a positive pitch input δ_θ produces a roll moment M_ϕ, but acts as a pitch moment M_θ due to the precession effect [12]. For clockwise rotating blades, this effect is taken into account by adding $\pi/2$ to the sine and cosine functions in the argument of the integral.

$$\begin{bmatrix} M_\phi \\ M_\theta \end{bmatrix} = \frac{n}{2\pi} \int_0^{2\pi} \int_0^{BR} r \begin{bmatrix} -\sin(\xi + \frac{\pi}{2}) \\ \cos(\xi + \frac{\pi}{2}) \end{bmatrix} d\mathbb{L}_m \, d\xi \tag{21}$$

Note that the above expression represents the average moment created by the rotor blades around a revolution. We assume that the rotor angular velocity is constant; thus $\xi = \Omega t$.

The lift element equation is similar to the flybar lift used in equation (14).

$$d\mathbb{L}_m = \frac{1}{2}\rho(\Omega r)^2 a\theta_{cyc} c \, dr \tag{22}$$

Geometrically, the cyclic pitch angle θ_{cyc} is affected by two different kinds of inputs as shown in Figure 4: a direct input by the pilot and an indirect input from the flybar. The geometry of the hub linkages indicate that θ_{cyc} will be the weighted sum of these two inputs. Aerodynamically, similar to the flybar, the angle of attack of the main blade will also be influenced by the ratio between the second element of the angular velocity vector of the main blade ω_{M2} and Ω [19].

To find the angular velocity of the main rotor blade ω_{M2}, we use a similar derivation method to that of the flybar case. The rotation matrix which relates the main blade position to the body coordinates of the

helicopter is denoted R_{BM}. Since the main blades do not flap, the pitch angle is zero. Also the roll angle is neglected.

$$R_{BM} = e^{(\hat{z}\times)(\xi)}\ e^{(\hat{y}\times)0}\ e^{(\hat{x}\times)0}$$

The rotation matrix relating the main blade frame to the inertial frame is: $R_{IM} = R_{IB}R_{BM}$. Similar to the flybar case, correction factors α_3 and α_4 were added to compensate for the simplified aerodynamics; they will also be determined in Section 4.

Therefore,

$$\begin{aligned}(\omega_M\times) &= R_{IM}^T\dot{R}_{IM} = R_{BM}^T(\omega_B\times)R_{BM} + R_{BM}^T\dot{R}_{BM}\\ \omega_{M2} &= -\omega_{B2}\sin\xi - \omega_{B1}\cos\xi\\ \theta_{cyc} &= \alpha_3\left(\frac{L_3}{L_1(L_2+L_3)}\delta_{cyc} + \frac{L_2L_4}{L_1(L_2+L_3)}\beta\right) - \alpha_4\frac{\omega_{M2}}{\Omega}\end{aligned}$$

The cyclic angle θ_{cyc}, and hence the pitch and roll moments, depend on the pitch and roll inputs through δ_{cyc} as well as on the flybar flapping angle β.

3.5.3 Yaw moment

The tail rotor on a helicopter is used to counteract the yaw moment created by the main rotor blades and to give a yaw directional control; thus, altering the amount of pitch on the tail rotor blades can create more or less total yaw moment for the helicopter. The motor yaw torque applied to the helicopter body by the motor is denoted τ_m and is modeled as proportional to the throttle/collective input δ_o.

$$\tau_m = -K_m \cdot \delta_o \tag{23}$$

The yaw command δ_ψ is the collective pitch of the tail rotor blades. There is no cyclic input for the tail rotor blades, only a collective pitch angle. The angular velocity of the tail rotor blades is related to the angular velocity of the main rotor blades through a constant K_Ω. This is realized by a simple gear connection or a pulley.

$$\Omega_T = K_\Omega \cdot \Omega$$

The thrust generated by the tail rotor is found in a similar manner to the thrust of the main rotor (20), replacing with the values from the tail rotor where appropriate.

$$T_T = \frac{n}{2}a_T c_T \rho\pi R_T^3\Omega_T^2\left(\frac{B^3}{3}\delta_\psi - \frac{B^2}{2}\lambda_T\right) \tag{24}$$

The subscripts T indicate that the values pertain to the tail rotor. The thrust of the tail rotor times the distance L_T between the main and tail rotor axes creates the yaw moment on the helicopter to counteract the spin of the blades.

In addition, there is a damping term in the equation for M_ψ due to the presence of an electronic gyro on the model helicopter. A simple linear model $K_g\omega_{B3}$ is used, although more sophisticated (PI controlled) gyros are now available [1].

$$M_\psi = T_T L_T - K_g\omega_{B3} \tag{25}$$

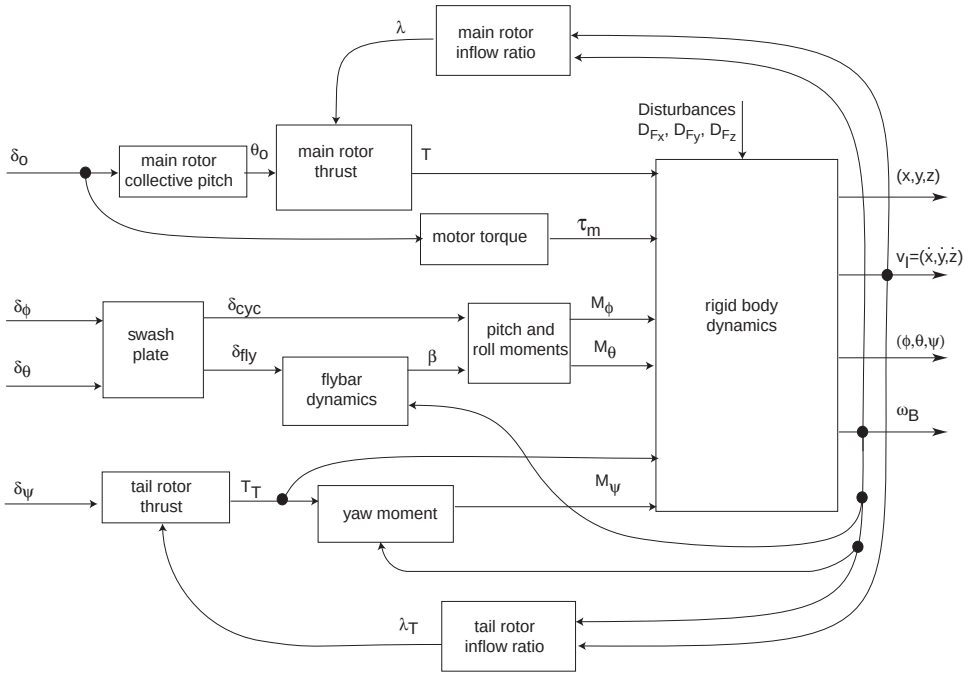

Figure 8: Block diagram of the helicopter model. The pilot inputs are $\delta_t, \delta_\phi, \delta_\theta, \delta_\psi$ and the outputs are the position, orientation, and velocity of the helicopter. Internal variables include the rotor orientation ξ the flybar flapping angle β, and the collective pitch angle θ_o.

3.6 Complete model

A block diagram of the complete mathematical model of the helicopter is shown in Figure 8. The inputs δ are the four stick positions of the model helicopter, and the outputs q are the rigid body positions, orientations, and velocities. Internal variables include the rotor orientation ξ, the flybar flapping angle β, and the collective pitch angle θ_o. The following set of differential and integral equations relate the input to output.

3.6.1 Main rotor collective pitch and motor torque

$$\ddot{\theta}_o + K_5\dot{\theta}_o + K_6\theta_o = K_4 \cdot \delta_o \tag{19}$$

$$\tau_m = -K_m \cdot \delta_o \tag{23}$$

3.6.2 Main and tail rotor thrusts

$$T = \frac{n}{2} ac\rho\pi R^3\Omega^2 \left(\frac{B^3}{3}\theta_o - \frac{B^2}{2}\lambda\right) \tag{20}$$

$$T_T = \frac{n}{2} a_T c_T \rho\pi R_T^3\Omega_T^2 \left(\frac{B^3}{3}\delta_\psi - \frac{B^2}{2}\lambda_T\right) \tag{24}$$

3.6.3 Rigid body dynamics

$$q = \begin{bmatrix} x_I & y_I & z_I & \dot{x}_I & \dot{y}_I & \dot{z}_I & \phi & \theta & \psi & \omega_{B1} & \omega_{B2} & \omega_{B3} \end{bmatrix}^T$$

$$\dot{q} = \begin{bmatrix} v_I \\ \frac{1}{m}\, R_{IB} f_B \\ \Upsilon\, \omega_B \\ \mathcal{I}^{-1}(\tau_B - \omega_B \times\, \mathcal{I}\, \omega_B) \end{bmatrix} \tag{5}$$

$$f_B = \begin{bmatrix} -D_{F_x} \\ -D_{F_y} - T_T \\ -D_{F_z} - T \end{bmatrix} + R_{IB}^T \begin{bmatrix} 0 \\ 0 \\ mg \end{bmatrix} \tag{3}$$

$$\tau_B = \begin{bmatrix} M_\phi \\ M_\theta - T\ell_r \\ M_\psi + \tau_m \end{bmatrix} \tag{4}$$

3.6.4 Pitch and roll moments

$$\begin{bmatrix} M_\phi \\ M_\theta \end{bmatrix} = \frac{nac\rho\Omega^2}{4\pi} \int_0^{2\pi} \int_0^{BR} \begin{bmatrix} -\sin(\xi + \frac{\pi}{2}) \\ \cos(\xi + \frac{\pi}{2}) \end{bmatrix} r^3 \theta_{cyc}\, dr\, d\xi \tag{21,22}$$

3.6.5 Yaw moment

$$M_\psi = T_T L_T - K_g \omega_{B3} \tag{25}$$

3.6.6 Swash plate

$$\delta_{cyc}(\xi) = -\frac{L_8}{L_9}(\delta_\theta \sin\xi + \delta_\phi \cos\xi) \tag{9}$$

$$\delta_{fly}(\xi) = -\frac{L_8}{L_9}(\delta_\theta \cos\xi - \delta_\phi \sin\xi) \tag{10}$$

3.6.7 Flybar dynamics

$$\omega_F = \begin{bmatrix} -\omega_{B3}\sin\beta + \cos\beta(\omega_{B1}\cos\xi' + \omega_{B2}\sin\xi') \\ \omega_{B2}\cos\xi' - \omega_{B1}\sin\xi' \\ \omega_{B3}\cos\beta + \sin\beta(\omega_{B1}\cos\xi' + \omega_{B2}\sin\xi') \end{bmatrix} + \begin{bmatrix} -\dot{\xi}'\sin\beta \\ \dot{\beta} \\ \dot{\xi}'\cos\beta \end{bmatrix} \tag{12}$$

$$-I_f\omega_{F1}\omega_{F3} + I_f\dot{\omega}_{F2} = n\int_{R_1}^{BR_2} r\,\frac{1}{2}\rho(\Omega r)^2 a\,(\frac{\alpha_1 L_7}{L_5 L_6}\delta_{fly} - \frac{\alpha_2\omega_{F2}}{\Omega})\,c_2\,dr \tag{14,15,17}$$

3.6.8 Main and tail rotor inflow ratios

$$\lambda = -\nu + \frac{v_i}{R\Omega}$$

$$\lambda_T = -\nu_T + \frac{v_{iT}}{R_T\Omega_T}$$

This set of system equations cannot be easily simulated because the flybar flapping angle β is a function of the rotor angle ξ, but the roll moment equation (21) cannot be solved directly unless β is expressed explicitly in terms of ξ. For simulation purposes, we approximate the flapping angle β as a sinusoidal function around each revolution:

$$\beta \approx \beta_{max} \cos(\xi - \xi_{max}) \tag{27}$$

where

$$\beta_{max} = \max_{0 \le \xi < 2\pi} \beta(\xi)$$
$$\xi_{max} = \arg \max_{0 \le \xi < 2\pi} \beta(\xi)$$

Using this approximation, the integrals in equation (21) can be computed analytically:

$$M_\phi = \frac{n\rho\Omega^2 acR^4B^4}{16L_1(L_2+L_3)} \left(\alpha_3 \left(\frac{L_3L_8}{L_9}\delta_\phi - L_2L_4\beta_{max}\cos\xi_{max} \right) - \alpha_4 L_1(L_2+L_3)\frac{\omega_{B1}}{\Omega} \right)$$
$$M_\theta = \frac{n\rho\Omega^2 acR^4B^4}{16L_1(L_2+L_3)} \left(\alpha_3 \left(\frac{L_3L_8}{L_9}\delta_\theta - L_2L_4\beta_{max}\sin\xi_{max} \right) - \alpha_4 L_1(L_2+L_3)\frac{\omega_{B2}}{\Omega} \right)$$

The system model can thus be reduced to a set of purely differential equations. A Simulink block diagram of the model has been built, and is used to compare the model with data taken as described in Section 4. In the simulation, the parameters β_{max} and ξ_{max} are determined for each rotor blade revolution. The β and ω_B terms in the M_ϕ and M_θ pitch and roll moments serve as damping terms in the rigid body equations, increasing the stability of the system from the double-integrator model. Figure 9 shows typically how β_{max} reacts to a pilot input.

In Section 4, we will use this mathematical model, together with experimental data, to estimate the physical parameters of the helicopter model along with the correction factors used in the model.

4 System Identification

The main purpose of the system identification is to find physical parameters used in the previous mathematical modeling section. Because of the complexity of the nonlinear model, the system identification is performed on a SISO basis, using specially-built stands to restrict the motion of the helicopter to one degree of freedom. The nonlinear equations were restricted to the SISO case and linearized around the hover condition to determine the continuous transfer functions for each degree of freedom. The coefficients of those transfer functions are the unknown parameters to be identified using standard linear system identification techniques.

The system identification is performed in the discrete-time domain using input-output data taken by flying the helicopter on the stands. The coefficients of a discrete-time transfer function of the same order as the continuous-time transfer function are identified using the direct least squares method. The transfer function is then converted into state space form, where the matrix logarithm method with zero-order hold is used to directly convert into the corresponding continuous-time transfer function. By keeping all the parameters numerical, we can avoid dealing with the nonlinear coefficients which arise when the continuous-time transfer function is converted into the equivalent discrete-time transfer function analytically.

A Polhemus sensor [21] is used to measure the position and orientation of the helicopter; full six degree-of-freedom information $(x_I, y_I, z_I, \phi, \theta, \psi)$ is available at 50Hz. As shown in Figure 10, the sensor consists of

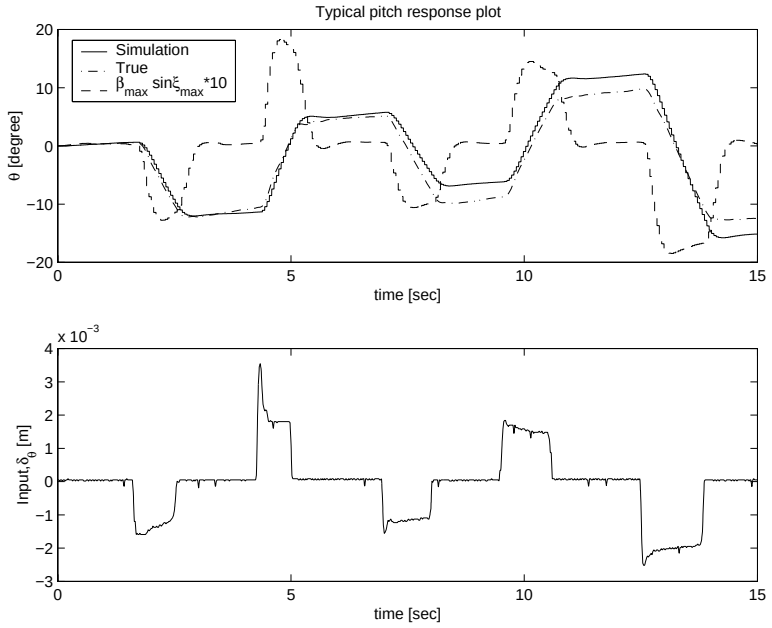

Figure 9: A typical pitch response simulation based on the nonlinear flybar model. Note that the flybar-disk tilt angle, $\beta_{max} \sin \xi_{max}$ tends to "subtract" the pilot input by lagging motion. It is magnified by $10\times$ for clarity.

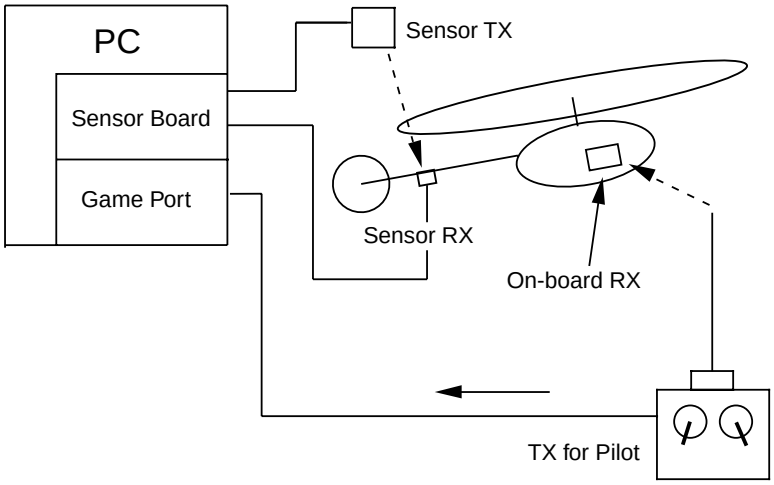

Figure 10: A sketch of the experimental setup for the system identification of the helicopter's physical parameters. The helicopter is controlled through the radio transmitter by a human pilot. The computer is used to record the input data from the transmitter and the output data from the sensor simultaneously.

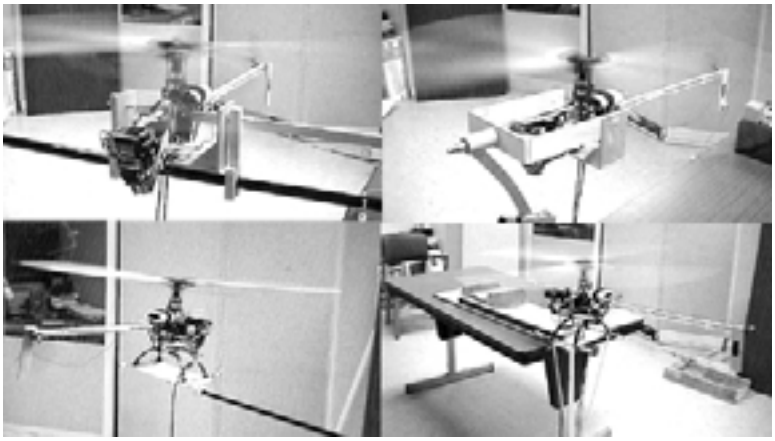

Figure 11: Separate identification was done for each degree of freedom. From top left, clockwise, they are pitch, roll, yaw, and heave identification.

a board connected to the PC's ISA slot, a transmitter, and a receiver. The transmitter is fixed to the earth and sends out a magnetic field via three orthogonal inductors. The receiver, fixed to the helicopter, senses the strength and the orientation of the magnetic field and sends this information back to the PC. The sensor has a static accuracy of 0.5 inches RMS for the x_I, y_I, and z_I position and 2 degrees RMS for the ϕ, θ, and ψ orientation. To obtain a reliable SISO ID result, we found that it is important to carefully design a stand which allows the helicopter to move in one direction for each ID session. Four different stands were used separately for each degree of freedom; they are shown in Figure 11. Each stand was constructed to be sturdy yet light-weight to minimize the influence of the stand dynamics. The input and output data are taken at 50 Hz for a total of approximately 40 sec duration for each degree of freedom.

Once the input-output data has been taken and stored for the isolated single DOF motion, the system identification algorithm is run to estimate the discrete-time transfer function coefficients. The initial condition of the system is also estimated using a least-squares method. The input data and the estimated transfer function are used to simulate the output data, and the simulated and actual output are compared. Ten independent identification sessions were run with similar results; the numerical results in Section 4.1 through 4.3 are the results of one of these sessions.

4.1 Pitch and Roll Identification

The main purpose of the pitch and roll identification is to find the inertia terms I_{xx} and I_{yy} used in equation (2), although the coefficients α_1 and α_2 must also be determined. The derivation will be done here for the roll equation; the pitch equations are similar. First, we substitute the approximation $\beta \approx \beta_{max}\cos(\xi - \xi_{max})$ from equation (27) into the roll-restricted equation for the flybar flapping angle β given by (18), resulting in the following expression:

$$-\cos\xi\ddot{\phi} + 2\Omega\sin\xi\dot{\phi} - \sin^2\xi\beta_{max}\cos(\xi-\xi_{max})\dot{\phi}^2 = P_1P_2\alpha_1\delta_\phi\sin\xi + \alpha_2P_1\beta_{max}\sin(\xi-\xi_{max}) + \frac{\alpha_2P_1}{\Omega}\dot{\phi}\cos\xi$$

where, to simplify the notation somewhat, the terms P_1 and P_2 are defined as follows:

$$P_1 = \frac{n\Omega^2}{8}\frac{\rho a c_2 (B^4 R_2^4 - R_1^4)}{I_f}$$
$$P_2 = \frac{L_7 L_8}{L_5 L_6 L_9}$$

Note that P_1 and P_2 can be determined by direct measurements of helicopter parameters. The lift curve slope a is taken to be 6 [12] and the flybar inertia I_f is computed using basic physics and the mass of the flybar.

Now, we collect terms in sine and cosine from the roll equation, resulting in

$$C_1 \cos(\xi - \xi_{max}) + C_2 \sin(\xi - \xi_{max}) = C_3 \cos\xi + C_4 \sin\xi \tag{28}$$

where, again, new notation has been introduced to simplify the expression:

$$C_1 = -\beta_{max} \sin^2 \xi \dot{\phi}^2$$
$$C_2 = -\alpha_2 P_1 \beta_{max}$$
$$C_3 = \ddot{\phi} + \frac{\alpha_2 P_1}{\Omega}\dot{\phi}$$
$$C_4 = -2\Omega\dot{\phi} + \alpha_1 P_1 P_2 \delta_\phi$$

Applying the trigonometric identity,

$$A_1 \cos\xi + A_2 \sin\xi = \sqrt{A_1^2 + A_2^2}\sin(\xi + \gamma)$$
$$\gamma = \arctan\frac{A_1}{A_2}$$

equation (28) can be rewritten as

$$\sqrt{C_1^2 + C_2^2}\sin\left(\xi - \xi_{max} + \arctan\frac{C_1}{C_2}\right) = \sqrt{C_3^2 + C_4^2}\sin\left(\xi + \arctan\frac{C_3}{C_4}\right)$$

which implies that the magnitude and phase terms on both sides of the equation should match:

$$C_1^2 + C_2^2 = C_3^2 + C_4^2$$
$$-\xi_{max} + \arctan\frac{C_1}{C_2} = \arctan\frac{C_3}{C_4}$$

Our system ID experiment suggests terms involving $\ddot{\phi}^2$, $\ddot{\phi}\dot{\phi}$, $\dot{\theta}^4$ and their coefficients are small in general. Based on this fact, solving for β_{max}^2 yields the following expression:

$$\beta_{max}^2 \approx \left(\frac{\alpha_1 P_2}{\alpha_2}\delta_\phi\right)^2 - 4\frac{\alpha_1 P_2 \Omega}{\alpha_2^2 P_1}\delta_\phi\dot{\phi} + \left(\frac{1}{\Omega^2} + \frac{4\Omega^2}{\alpha_2^2 P_1^2}\right)\dot{\phi}^2$$

Neglecting $1/\Omega^2$, which is also small, we get a perfect square, and use the approximation

$$\beta_{max} \approx \frac{\alpha_1 P_2}{\alpha_2}\delta_\phi - \frac{2\Omega}{\alpha_2 P_1}\dot{\phi}$$

Next, we need to solve for ξ_{max}. Inspecting the magnitudes and signs of C_1–C_4, we can determine that, for roll motion,

$$\arctan\frac{C_1}{C_2} \approx \pi$$
$$\arctan\frac{C_3}{C_4} \approx 0$$

and therefore,

$$\xi_{max} \approx \pi$$

We now substitute β_{max} and ξ_{max} into the expression for M_ϕ from (21),

$$M_\phi = \left(\frac{\alpha_3 P_3 L_3 L_8}{L_9} + \frac{\alpha_1 \alpha_3}{\alpha_2} P_2 P_3 L_2 L_4\right)\delta_\phi - \left(\frac{2\alpha_3 P_3 L_2 L_4 \Omega}{\alpha_2 P_1} + \frac{\alpha_4 P_3 L_1 (L_2 + L_3)}{\Omega}\right)\dot{\phi} \tag{29}$$

where

$$P_3 = \frac{n\rho ac\Omega^2 R^4 B^4}{16 L_1 (L_2 + L_3)}$$

can be measured directly.

We now have an analytic coefficients for a simplified linear transfer function describing SISO roll dynamics:

$$\frac{\Phi(s)}{\delta_\phi(s)} = \frac{\left(\frac{\alpha_3 P_3 L_3 L_8}{L_9} + \frac{\alpha_1 \alpha_3}{\alpha_2} P_2 P_3 L_2 L_4\right)\frac{1}{I_{xx}}}{s\left(s + \left(\frac{2\alpha_3 P_3 L_2 L_4 \Omega}{\alpha_2 P_1} + \frac{\alpha_4 P_3 L_1 (L_2 + L_3)}{\Omega}\right)\frac{1}{I_{xx}}\right)} \tag{30}$$

We now have a transfer function with parameters to be identified by comparing with a numerical identification. However, the expression contains not only I_{xx}, but also α. We therefore need to determine appropriate α before finding I_{xx}. This task is not straightforward because α, I_{xx}, I_{yy} and the 6DOF simulation all depend on each other. One can nevertheless find a suitable set of parameters to obtain a reasonable solution.

An ID was carried out to obtain a discrete transfer function $H_\phi(z)$ and $H_\theta(z)$, with 2 poles and 2 zeros. Before ID, the roll output data was filtered using a 1st order low-pass Butterworth filter with the cut-off frequency at 1.5 Hz.

$$H_\phi(z) = \frac{0.559 z^2}{z^2 - 1.81z + 0.816}$$

This transfer function is then converted into an equivalent continuous transfer function $H_\phi(s)$, using a matrix logarithm method with zero order hold. Ignoring small coefficients for the numerator and assuming the pole at $s = -0.503$ to be at the origin,

$$\frac{\Phi(s)}{\delta_\phi(s)} = \frac{0.559 s^2 + 45.8 s + 1540}{s^2 + 10.2 s + 4.85} \approx \frac{1540}{s(s + 9.65)}$$

We apply the same technique for the pitch motion; the pitch output data was filtered using a 1st order low-pass Butterworth filter with the cut-off frequency at 1.0 Hz.

$$H_\theta(z) = \frac{0.234 z^2}{z^2 - 1.92z + 0.922}$$

$$\frac{\Theta(s)}{\delta_\theta(s)} = \frac{0.234 s^2 + 18.2 s + 610}{s^2 + 4.04 s + 0.946} \approx \frac{610}{s(s + 3.80)}$$

The inertia terms can now be calculated by applying the identified numerical values into (30). However, we now have 2 equations for 1 unknown and they do not necessary yield a single solution. We therefore use averaged values for each motion, to determine

$$I_{xx} = 0.137\ kg.m^2$$
$$I_{yy} = 0.221\ kg.m^2$$

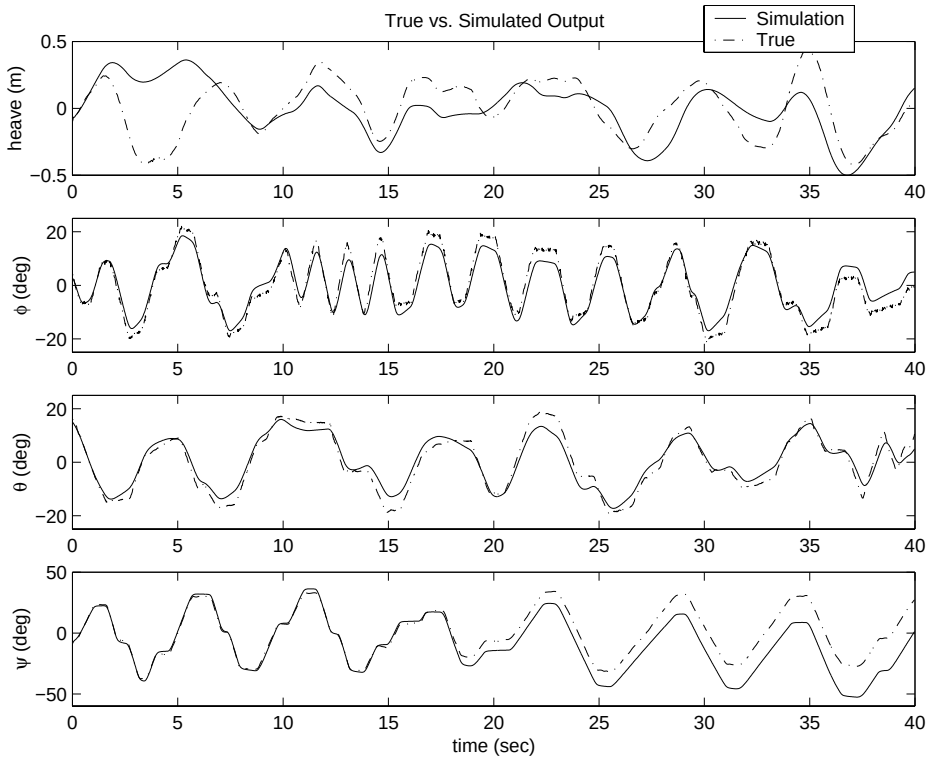

Figure 12: The comparison between the simulated outputs based on the identified discrete time transfer functions and the actual outputs from the experiment, given the identical input command history separately. The initial values for the simulation was also determined with least squares method using the first 50 points from the experiment.

Meanwhile, a reasonable match is achieved between the true data and $H(z)$, as shown in Figure 12. For the roll motion ID, the mean-squared error between the actual output ϕ_a and the simulated output ϕ_s from the estimated transfer function is computed as follows:

$$\text{RMS Error} = \sqrt{\frac{1}{N}\sum_{i=1}^{N}(\phi_a(i) - \phi_s(i))^2}$$

Typical values for this error are on the order of a few degrees, which is of the same order as the accuracy of the sensor.

To determine the validity of the single-axis identification, an experiment was performed in which both pitch and roll motions were commanded by the pilot. The input-output data was collected, and the input data was used with the single-input transfer functions to simulate both the pitch and roll outputs. The results from this experiment are given in Figure 13. There is some coupling between the pitch and roll motions, but it does not overwhelm the dominant single-input effects. A sampling of the mean-squared errors is given in Table 1.

4.2 Yaw Identification

By comparing $H_\psi(z)$ with a second order yaw dynamic model from equation (2), we can obtain parameters such as I_{zz} and K_g which are uniquely related to the yaw dynamics. We first rewrite the yaw dynamic

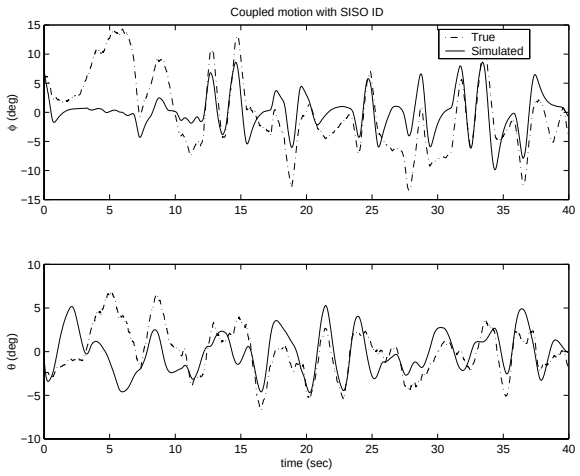

Figure 13: The system identification result is applied to the pitch and roll motion simultaneously. The figure shows some coupled responses through the discrepancy between the true and the simulated result.

Table 1: A sampling of the mean-squared errors between the actual and simulated outputs using the identified transfer functions $H_\phi(z)$, $H_\theta(z)$, $H_z(z)$, and $H_\psi(z)$. Although the errors are slightly larger in the coupled experiment, they are still small enough to give some degree of confidence in the identified transfer function.

experiment	RMS error
pitch SISO	2.9 degree
roll SISO	3.3 degree
yaw SISO	13 degree
heave SISO	0.22 m
pitch coupled	2.9 degree
roll coupled	5.4 degree

equation for hover by considering the yaw moment input M_ψ and yaw angle output ψ only.

$$I_{zz}\dot{\omega}_{B3} = M_\psi - \tau_m = M_{\delta_\psi} - K_g\omega_{B3} - \tau_m$$

where we have defined M_{δ_ψ} as $T_T L_T$. For the reaction moment τ_m,

$$\tau_m = -K_m \cdot \delta_o$$

the proportional constant K_m can be found by directly measuring τ_m using a small spring scale with respect to several different values of δ_o, and results in

$$K_m = 0.178 \text{ N.m/deg}$$

We then linearize about hover, using the reference value $\delta_\psi = 0$ when there is no yaw moment, to get

$$I_{zz}\ddot{\psi} = M_{\delta_\psi} - K_g\dot{\psi}$$

$$\frac{\Psi(s)}{M_{\delta_\psi}(s)} = \frac{1/I_{zz}}{s(s + K_g/I_{zz})}$$

Before ID, the output data was filtered using a 5th order low-pass Butterworth filter with the cut-off frequency at 5 Hz. After using the identification procedure similar to the roll and pitch case, and ignoring the near-infinite zero at $s = -104$ and assuming the pole at $s = -0.0245$ to be at the origin,

$$\frac{\Psi(s)}{M_{\delta_\psi}(s)} = \frac{0.289s + 30.1}{s^2 + 12.3s + 0.301} \approx \frac{30.1}{s(s + 12.3)}$$

We can then find the parameters,

$$I_{zz} = 0.0332 \; kg.m^2$$
$$K_g = 0.408 \; kg.m$$

Based on the equation (25), we first need to find the relationship between δ_ψ and M_{δ_ψ} to be able to use the yaw dynamics model given above. We ignore the effect of λ_T, then directly measure the yaw moment per several different values of δ_ψ using a simple spring scale. That is,

$$M_{\delta_\psi} \approx 0.0474 \text{ [N.m/deg] } \delta_\psi$$

4.3 Heave Identification

We can also simplify the heave motion dynamic model from equations (2) and (20) for the hovering condition. Selecting a nominal value of θ_o at hover, gives the equation

$$\ddot{z} + K_1\dot{z} + K_2 z = K_3\theta_o \tag{31}$$

where,

$$K_1 = \text{coefficient for simplified } \lambda$$
$$K_2 = \text{coefficient for ground effect}$$
$$K_3 = \frac{nac\rho\pi R^3\Omega^2 B^3}{6m}$$

Table 2: List of parameters identified using the system identification method for ten independent runs. Average and standard deviation values are reported.

Parameter	Average values with standard deviation
I_{xx}, Roll Inertia	0.137 ± 0.0228 $[kg \cdot m^2]$
I_{yy}, Pitch Inertia	0.221 ± 0.0478 $[kg \cdot m^2]$
I_{zz}, Yaw Inertia	0.0323 ± 0.00234 $[kg \cdot m^2]$
K_g, Gyro Gain	0.400 ± 0.0104 $[kg \cdot m]$
K_1	0.886 ± 0.0954 $[N.sec.kg^{-1}.m^{-1}]$
K_2	1.12 ± 0.250 $[N.kg^{-1}.m^{-1}]$
K_3K_4	442000 ± 73200 $[N^2.kg^{-2}.deg^{-2}]$
K_5	27.7 ± 1.20 $[N.sec.kg^{-1}.deg^{-1}]$
K_6	5760 ± 302 $[N.kg^{-1}.deg^{-1}]$

Since our identification was done near-ground environment, the approximated ground effect, $K_2 z$ was not negligible. Further investigations indicated that there was significant mechanical compliance in the collective pitch control system, and equation (19) was added to the system model.

$$\frac{\Theta_o(s)}{\delta_o(s)} = \frac{K_4}{s^2 + K_5 s + K_6}$$

Combining the equation (19) and (31), we arrived at a forth order continuous-time transfer function,

$$\frac{Z(s)}{\delta_o(s)} = \frac{K_3 K_4}{(s^2 + K_1 s + K_2)(s^2 + K_5 s + K_6)}$$

Similar to the yaw case, we identified the discrete transfer function $H_z(z)$ with 4 poles and 4 zeros, then converted this into a continuous transfer function. Before ID, the input data was filtered using a 3rd order low-pass Butterworth filter with the cut-off frequency at 5 Hz. The output data was filtered with 1st order at 10 Hz. Ignoring the small coefficients in the numerator,

$$\frac{Z(s)}{\delta_o(s)} = \frac{-0.887s^3 + 129s^2 - 10131s + 326000}{s^4 + 29.6s^3 + 5030s^2 + 4740s + 5070} \approx \frac{326000}{(s^2 + 0.942s + 1.01)(s^2 + 28.7s + 5004)}$$

4.4 Identification Summary

Note that one could simply use the identified transfer functions from the roll, pitch, yaw and heave identification directly without going through the simplification presented in the last sections. However, those ignored or neglected poles and zeros basically represent unmodelled dynamics not included in equation (2). Therefore, those terms do not guarantee the usefulness for all operating conditions.

Standard deviations for identified parameters were determined by repeating the identification session 10 times. Input and output data were collected for 10 minutes then divided into 10 sections for 10 different ID sessions. Table 2 summarizes all the parameters identified.

4.5 Model Validation

By comparing equation (2) with a 6DOF data collected while flying the helicopter, we can visualize how well the mathematical model predicts the actual system. Figure 14 shows a reasonable agreement between the 6DOF mathematical model and the experimental result. Only the initial positions were matched at the beginning of the simulation. Initial velocities were all assumed zero. One cannot approximate the initial conditions using least square technique due to the feedback nature of the simulation model. The helicopter initially took off from the ground then was brought to a hover. Since the take-off dynamics are not included in the model, we cannot use the take-off point as the initial condition, but use an estimated hover point as the initial condition.

Four degrees of freedom (heave, roll, pitch, and yaw) are shown. The translational motions (x and y) are not shown due to poor agreement between the simulation and the true data. The model for these two motions are directly dependent on the pitch, yaw, and roll motion simulation data. We believe an accurate open-loop simulation of x and y motion is not possible through a mathematical model due to the helicopter's sensitivity to the disturbances. In fact, one cannot obtain two identical trajectories of the helicopter even if identical inputs are applied to the actual helicopter. This is one of the reasons why helicopter requires a closed loop controller for a stable maneuvering. Evidently, for heave and yaw motion, the simulation shows significant amount of drift after about 10 seconds.

The same parameters used for Figure 14 were also applied to two different experiments and the comparison is shown in Figures 15 and 16. Reasonable agreement was obtained, proving that the estimation routine and the parameters obtained from Section 4 are valid for different experiments within the given flight envelope.

This paper is primarily concerned with understanding the flybar dynamics, and all of the aerodynamic model is based on a simple, idealized 2-D model. This limited the actual performance of the mathematical model and required using correction factors. The drag forces along the x, y, and z directions are difficult to estimate due to complex aerodynamic interactions between the rotor, fuselage, and ground effect. Other disturbances such as air circulation due to rotor blast in the lab environment are neglected. However, as shown by the experimental identification, this model captures the dominant dynamic effects in the model helicopter's motion, and as such, will be useful for both control design and trajectory planning for this system.

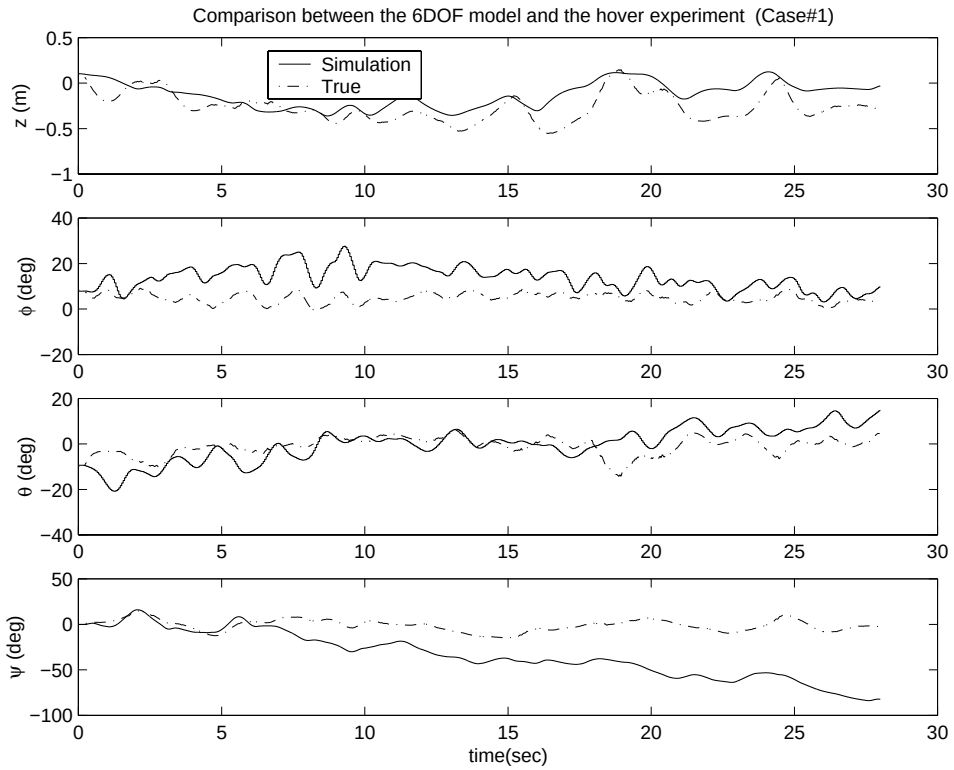

Figure 14: The comparison between the simulated outputs based on the 6DOF nonlinear model and the actual outputs from the experiment, given the identical input command history separately.

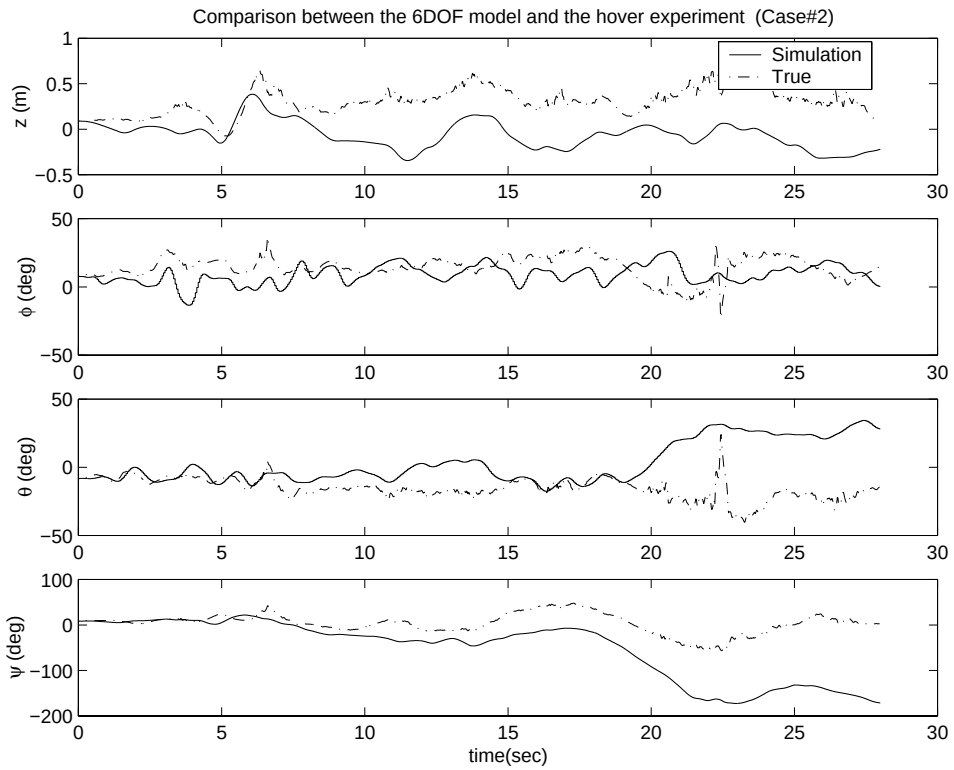

Figure 15: Another 4DOF simulation.

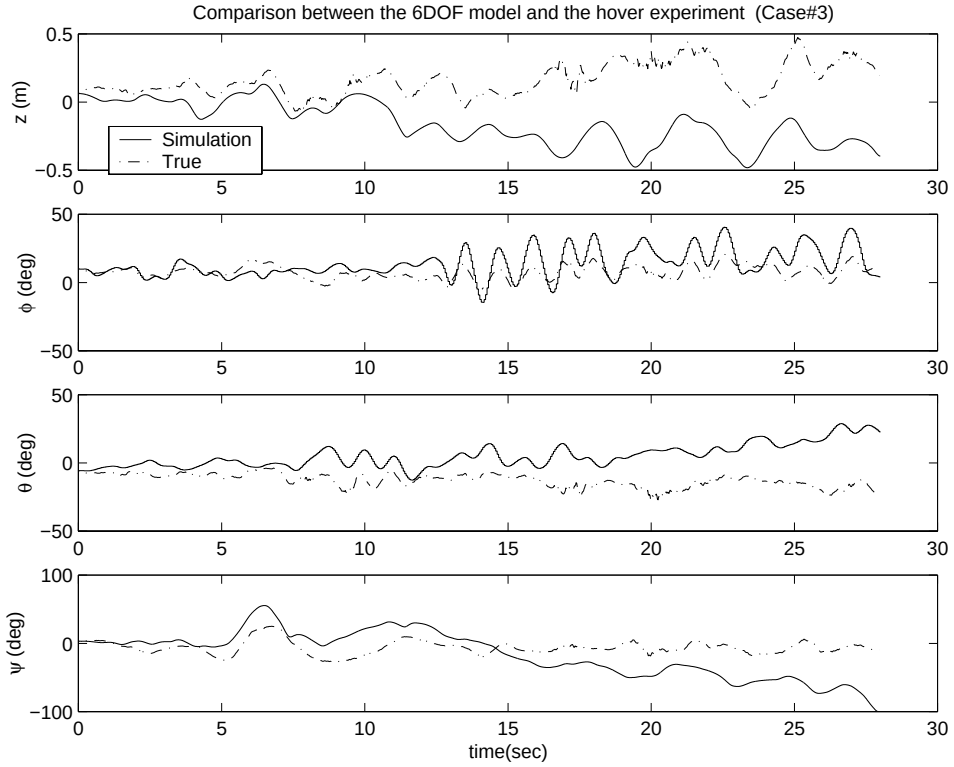

Figure 16: Another 4DOF simulation.

The following are the values used for the simulation.

a	6
α	[0 3 0.3 1]
B	0.97
c	0.044 m
c_2	0.038 m
g	9.8 m/s^2
I_f	0.00128 kg·m^2
I_{xx}	0.137 kg·m^2
I_{yy}	0.221 kg·m^2
I_{zz}	0.0323 kg·m^2
K_g	0.400 kg·m
K_m	0.178 N·m/deg
K_1	0.886 $N.sec.kg^{-1}.m^{-1}$
K_2	1.12 $N.kg^{-1}.m^{-1}$
K_3K_4	442000 $N^2.kg^{-2}.deg^{-2}$
K_5	27.7 $N.sec.kg^{-1}.deg^{-1}$
K_6	5760 $N.kg^{-1}.deg^{-1}$
L_T	0.635 m
L_1	0.0190 m
L_2	0.0119 m
L_3	0.0098 m
L_4	0.0250 m
L_5	0.0177 m
L_6	0.0110 m
L_7	0.0234 m
L_8	0.0175 m
L_9	0.0266 m
m	1.36 kg
R	0.508 m
R_1	0.15 m
R_2	0.21 m
ρ	1.2 kg/m^3
Ω	1190 RPM

5 Conclusions

In this paper, we have derived a complete mathematical model for a model-scale helicopter, experimentally identified the key parameters of the model, and verified the model through simulation. The main contribution of the work is the new model of interaction between the flybar and the main rotor blade. A flybar is typically used on model-scale helicopters to augment the stability and aid in actuation. Understanding the dynamics of the rotor hub is the essential part of the modeling of a model helicopter. A controller design based on the

model presented should be a more sounding controller design strategy than that of based on the model for full scale helicopter.

The result of this work will be of interest to researchers and developers working in the increasingly important area of small, autonomous aerial vehicles.

6 Nomenclature

a	main rotor lift slope
a_T	tail rotor lift slope
B	tip loss factor
c, c_2, c_T	main/flybar/tail blade chord length
$D_{F_{x,y,z}}$	fuselage profile drag forces along body coordinates
dL, dL_m	differential lift elements for flybar and main rotor blade
dr	differential length elements for flybar and main rotor blade
f_B	external force applied along body coordinates
g	gravitational acceleration
h_r	distance between rotor disk and CG, parallel to rotor axis
$\widehat{I}$	rotational inertia matrix of flybar
$I_{3\times3}$	3x3 identity matrix
I_f	flybar moment of inertia in flapping
$I_{xx,yy,zz,xz}$	fuselage rotational moments of inertia
$\mathcal{I}$	rotational inertia matrix of helicopter
K_g	gyro gain for tail rotor
K_m	motor reaction torque gain
K_Ω	proportional constant relating Ω to Ω_T
$K_1 \ldots K_6$	proportional constants used for identification
ℓ_r	distance between rotor axis and CG, perpendicular to rotor axis
L_T	distance between tail rotor axis and CG
$L_1 \ldots L_9$	linkage lengths in rotor hub assembly
m	helicopter total mass
m_F	Flybar mass per length
$M_{\phi,\theta,\psi}$	net moments on helicopter
M_{δ_ψ}	yaw moment due to pilot input
n	Number of main/flybar/tail blades
r	position along the main rotor blade
R	length of main rotor blade
R_T	length of tail rotor blade
R_1	distance between rotor axis and flybar tip
R_2	distance between rotor axis and flybar root
$R_{IB,BF,IF}$	rotation matrices between Inertial, Body, and Flybar frames
$R_{IB,BM,IM}$	rotation matrices between Inertial, Body, and main rotor frames
T	net thrust generated by rotor
T_m	torque applied by motor
T_T	tail rotor translational lift force
v_i	induced air velocity through rotor disk
v_I	helicopter velocity with respect to inertia coordinates
$v_B, \dot{v}_B$	linear body velocity and acceleration
x_B, y_B, z_B	helicopter position in body coordinates
x_I, y_I, z_I	helicopter position in inertia coordinates
β	flybar flapping angle
β_{max}	maximum value of flybar flapping angle
δ_{cyc}	cyclic input displacement
δ_{fly}	cyclic input to flybar
$\delta_\theta, \delta_\phi, \delta_\psi$	roll, pitch, and yaw command input
δ_o	throttle/collective command input
θ_{fly}	angle of attack of flybar
θ_o	collective pitch angle of main rotor blades
θ_{cyc}	cyclic pitch angle of a main rotor blade
λ	inflow ratio for main rotor
λ_T	inflow ratio for tail rotor
ρ	air density
τ_B	external moment applied along body coordinates
τ_F	moment applied to flybar
ϕ, θ, ψ	helicopter angular position
$\omega_B, \dot{\omega}_B$	angular velocity and acceleration of helicopter
ω_F	angular velocity of flybar
Ω	main rotor angular velocity
Ω_T	tail rotor angular velocity
Υ	transformation matrix between ω_B and $[\dot{\phi}, \dot{\theta}, \dot{\psi}]^T$
ξ	main blade orientation angle
ξ_{max}	main blade orientation angle where β_{max} is detected

References

[1] Arcamax Control Systems Inc. 150 E. Pleasant Hill Rd. Suite 174 Carbondale, IL 62901. *Arcamax PI gyro.*

[2] Aveox Inc. 31324 Via Colinas Suite-103 Westlake Village, CA 91362. *1406/2Y Brushless Motor.*

[3] A. Azuma. Dynamic analysis of the rigid rotor system. *Journal of Aircraft*, 4(3), 1967.

[4] A. Bramwell. *Helicopter Dynamics.* Halsted Press, 1976.

[5] Aerial Robotics Competition. As part of the association for unmanned vehicle systems international. The home page is at http://avdil.gtri.gatech.edu/AUVS/IARCLaunchPoint.htm.

[6] T. Ellenrieder and P. Brinson. The dynamic induced velocity field of a model rotor in hover condition. *The Aeronautical Journal*, pages 331–335, June/July 1998.

[7] K. Furuta, Y. Ohyama, and O. Yamano. Dynamics of rc helicopter and control. *Mathematics and Computers in Simulation XXVI*, pages 148–159, 1984.

[8] Hobby Lobby Intl., 5614 Franklin Pike Cr - Brentwood, TN 37027. *Ikarus ECO electric helicopter.*

[9] R. Hostetler. *RAY's complete helicopter manual.* R/C modeler corporation, 1991.

[10] E. Johnson and P. DeBitetto. Modeling and simulation for small autonomous helicopter development. In *Proceedings of the AIAA Modeling and Simulation Technologies Conference*, pages 41–51, 1997.

[11] E. Johnson, P. DeBitetto, C. Trott, and M. Bosse. The 1996 MIT/Boston Univ/Draper Lab autonomous helicopter system. In *Proceedings of the 15th AIAA/IEEE Digital Avionics Systems Conference*, pages 381–386, 1996.

[12] W. Johnson. *Helicopter Theory.* Dover Publications, Inc., 1980.

[13] T. Koo and S. Sastry. Output Tracking Control Design of a Helicopter Model Based on Approximate Linearization". In *Proceedings of the IEEE Conference on Decision and Control*, 1998.

[14] E. Lee, H. Shim, H. Park, and K. Lee. Design of hovering attitude controller for a model helicopter. In *In Proceedings of Society of Instrument and Control Engineers*, pages 1385–1389, August 1993.

[15] J. Montgomery and G. Bekey. Learning Helicopter Control Through "Teaching by Showing". In *Proceedings of the IEEE Conference on Decision and Control*, 1998.

[16] J. Morris, M. Nieuwstadt, and P. Bendotti. Identification and control of a model helicopter in hover. In *Proceedings of the American Control Conference*, volume 2, pages 1238–1242, 1994.

[17] R. Murray, Z. Li, and S. Sastry. *A Mathematical Introduction to Robotic Manipulation.* CRC Press, 1994.

[18] Y. Okuno, K. Kawachi, A. Azuma, and S. Saito. Analytical prediction of height-velocity diagram of a helicopter using optimal control theory. *AIAA Journal of Guidance, Control, and Dynamics*, 14(2):453–459, 1991.

[19] G. Padfield. *Helicopter Flight Dynamics.* Blackwell Science Ltd, 1996.

[20] T. Pallett. Real-time helicoper flight control. Master's thesis, School of Electrical Engineering, Purdue University, August 1991.

[21] Polhemus Incorporated, P.O. Box 560, Colchester, VT 05446. *3SPACE User's Manual*, December 1993.

[22] M. Rohlfs. Identification of non-linear derivative models from BO-105 flight test data. *The Aeronautical Journal*, 102(1011):1–8, January 1998.

[23] D. Schlüter. *Schlüter's Radio Controlled Helicopter Manual*. Argus Books Ltd., 1981.

[24] R. Shevell. *Fundamentals of Flight*. Prentice-Hall, Inc., 1989.

[25] M. Sugeno. Fuzzy hierarchical control of an unmanned helicopter, 1994. available at ftp://ftp.cs.arizona.edu/japan/kahaner.reports/sugeno.94.

[26] D. Teare, P. FitzSimons, and B. Tongue. Time domain parameter identification techniques applied to the UH-60A black hawk helicopter. *Vetica*, 13(3):393–401, 1989.

[27] M. Weilenmann and H. Geering. Test bench for rotorcraft hover control. *AIAA Journal of Guidance, Control, and Dynamics*, 17(4):729–736, 1994.

[28] X. Zhu and M. Nieuwstadt. The Caltech helicopter control experiment. *CDS Technical Report 96–009*, 1996.